JACS
JOURNAL OF THE AMERICAN CHEMICAL SOCIETY

Article

Modulation of Water Vapor Sorption by a 4th Generation Metal-Organic Material with a Rigid Framework and Self-Switching Pores

Shi-Yuan Zhang, Stephanie Jensen, Kui Tan, Lukasz Wojtas, Matthew Roveto, Jeremy Cure, Timo Thonhauser, Yves J. Chabal, and Michael J. Zaworotko

J. Am. Chem. Soc., **Just Accepted Manuscript** • DOI: 10.1021/jacs.8b07290 • Publication Date (Web): 08 Sep 2018

Just Accepted

ACS Publications

is published by the American Chemical Society. 1155 Sixteenth Street N.W., Washington, DC 20036

Modulation of Water Vapor Sorption by a 4th Generation Metal-Organic Material with a Rigid Framework and Self-Switching Pores

Shi-Yuan Zhang[†], Stephanie Jensen[§], Kui Tan[‡], Lukasz Wojtas[‖], Matthew Roveto[§], Jeremy Cure[‡], Timo Thonhauser[§], Yves J. Chabal[‡], and Michael J. Zaworotko[†,*]

[†] Department of Chemical Science, Bernal Institute, University of Limerick, Limerick, Republic of Ireland

[‡] Department of Materials Science and Engineering, University of Texas at Dallas, Richardson, TX 75080, USA

[§] Department of Physics and Center for Functional Materials, Wake Forest University, Winston-Salem, NC 27109, USA

[‖] Department of Chemistry, University of South Florida, Tampa, FL 33620, USA

ABSTRACT: Hydrolytically stable adsorbents are needed for water vapor sorption related applications; however, design principles for porous materials with tunable water sorption behavior are not yet established. Here, we report that a platform of 4th generation metal-organic materials (MOMs) with rigid frameworks and self-switching pores can adapt their pores to modulate water sorption. This platform is based upon the hydrolytically stable material CMOM-**3S**, which exhibits **bnn** topology and is comprised of rod building blocks based upon *S*-mandelate ligands, 4,4-bipyridine ligands and extra-framework triflate anions. Isostructural variants of CMOM-**3S** were prepared using substituted *R*-mandelate ligands and exhibit diverse water vapor uptakes (20-67 cc/g) and pore filling pressures (P/P_0, 0.55-0.75). $[Co_2(R\text{-4-Cl-man})_2(bpy)_3](OTf)$ (**33R**) is of particular interest because of its unusual isotherm. Insight into the different water sorption properties of the materials studied was gained from analysis of *in situ* vibrational spectra, which indicate self-switching pores via perturbation of extra-framework triflate anions and mandelate linker ligands to generate distinctive water binding sites. Water vapor adsorption was studied using *in situ* differential spectra that reveal gradual singlet water occupancy followed by aggregation of water clusters in the channels upon increasing pressure. First-principles calculations identified the water binding sites and provide structural insight on how adsorbed water molecules affect the structures and the binding sites. Stronger triflate hydrogen bonding to the framework along with significant charge redistribution were determined for water binding in **33R**. This study provides insight into a new class of 4th generation (self-switching pores) MOM and the resulting effect upon water vapor sorption properties.

INTRODUCTION

Control over water vapor sorption processes in microporous solids is relevant for applications such as heat pumps,[1] dehumidification,[2] moisture harvesting,[3] water purification,[4] etc.[5] Water capture by porous solids requires water condensation occurring at low relative pressure ($P/P_0 < 0.1$) with a steep uptake.[6] On the other hand, materials for CO_2 capture and toxic gas removal should exhibit minimal water vapor uptake at saturated pressure ($P/P_0 = 1$) since water vapor can act as a strong competitor.[7] In terms of water capture and release, traditional sorbents such as silica gels and zeolites are limited by their very strong affinity for water vapor and high energy footprint for recycling.

Porous crystalline metal-organic materials, MOMs, such as porous coordination polymers, PCPs,[8] and metal-organic frameworks, MOFs,[9] are highly promising materials in this context because they can exhibit extra-high surface area and their modular nature can lead to fine-tuning of pore size and pore chemistry. Such fine-tuning can afford platforms of related materials that enable systematic study of structure-function relationships of relevance to, for example, gas storage and separation.[10] Kitagawa has classified porous PCPs and MOFs into three generations of materials (Scheme 1):[11] 1st generation materials collapse after guest removal and are rendered non-porous; 2nd generation MOFs possess framework rigidity upon guest removal and usually exhibit Type I adsorption isotherms; 3rd generation MOFs were classified as "soft" since their frameworks are flexible and characterised by 'stepped' or 'S-shaped' isotherms[12]. Most recently, Su *et al.*[13] defined 4th generation materials as porous materials with "modifiable" pore size and chemistry through post-synthetic modification[14] (Scheme 2a). Kitagawa has recently proposed that 4th generation MOFs also include MOFs affected by material anisotropy and any number of defects, including solid solutions and multivariate (MTV) MOFs (Scheme 2b and c).[12f] A different type of 4th generation material would be one that combines a rigid framework with self-switching pores that can adapt to a particular guest through extra-framework counterions that are free to move within the pore space (Scheme 2d) or flexible ligand substituents (Scheme 2e). Such 4th generation "hard-soft" materials might therefore, at least in principle, combine the advantages of 2nd and 3rd generation MOFs while eliminating the drawbacks: a) retention of topology and structural integrity during gas or vapor adsorption; b) soft pore surfaces that respond to external stimuli, leading to diverse sorption profiles; c) most importantly, the ability of self-adapt pore size and pore chemistry to accommodate different guest species.

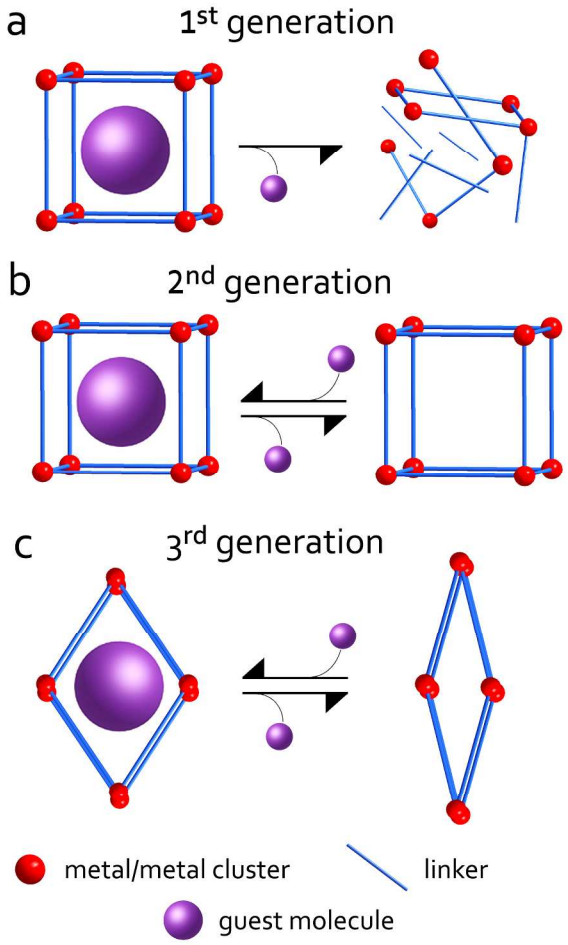

Scheme 1. Classification of PCPs and MOFs: (a) 1st generation materials collapse after guest removal; (b) 2nd generation MOFs possess framework rigidity upon guest removal and usually exhibit Type I adsorption isotherms; (c) 3rd generation MOFs are flexible and characterized by 'stepped' or 'S-shaped' isotherms.

We report herein that CMOM-**3S**, a chiral porous MOM that is hydrolytically stable, is the parent of a platform of related CMOM materials that exemplify 4th generation porous materials in that they can modulate water vapor sorption profiles such as water uptake and the relative pressure at which the pore filling occurs. CMOM-**3S** exhibits **bnn** topology and is a variant of CMOM-**1S**, $[Co_2(man)_2(bpy)_3](NO_3)_2$ (man = (*S*)-mandelate, **1S**, or (*R*)-mandelate, **1R**, bpy = 4,4'-bipyridine). CMOM-**3S** features 1D periodic chiral channels decorated with triflate anions (OTf^-).[15] CMOM-3S is a 4th generation prototype that exhibits an adaptable internal surface that can serve as a crystalline sponge[16] for various phenyl alcohols and nitriles.[15b] In addition, CMOM-**3S** offers exceptional thermal and hydrolytic stability and crystallinity, which enables it to be used for chiral purification and enantiomer identification. A series of CMOM-**3S** analogs generated using monosubstituted mandelate linkers was prepared and herein we report their structures, water vapor sorption properties and insight into these properties gained from first-principles modelling and spectroscopy.

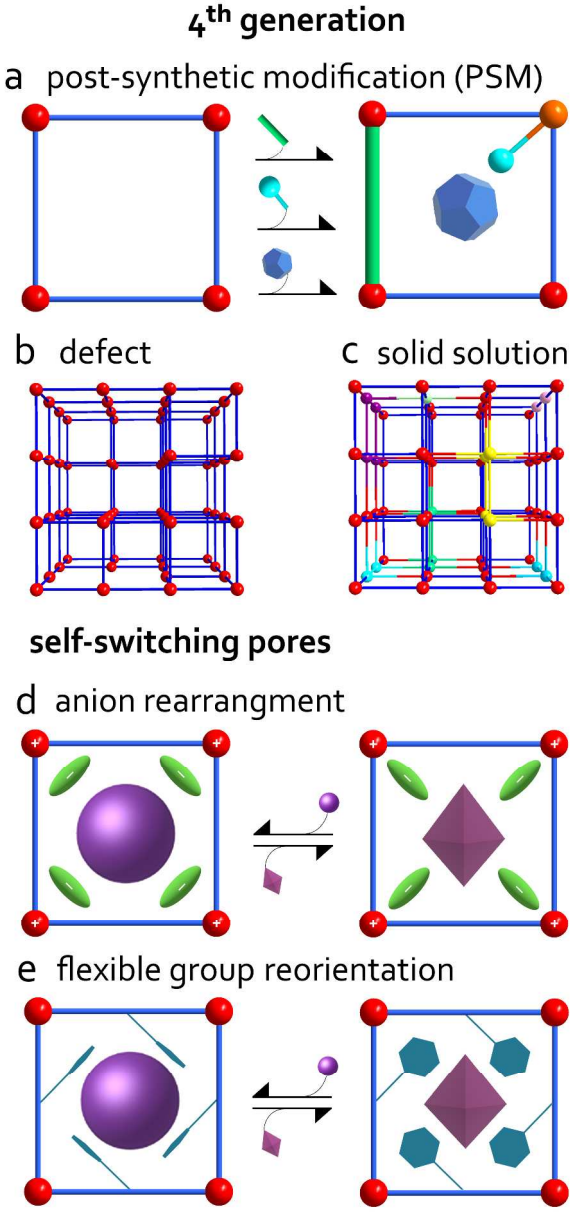

Scheme 2. 4th generation porous materials are modifiable using (a) post-synthetic approaches that chemically modify their pore structure or they are complex systems that (b) contain defects or (c) are non-stoichiometric (solid solution). A different type of 4th generation porous materials exhibits rigid frameworks with self-switching pores that adapt to a particular guest through (d) rearrangement of extra-framework counterions or (e) reorientation of flexible ligand substituents.

Four new isostructural variants of CMOM-**3S** were prepared (Figure 1): $[Co_2(S\text{-man})_2(bpy)_3](OTf)_2$ (**3S**); $[Co_2(R\text{-2-Cl-man})_2(bpy)_3](OTf)_2$ (**13R**); $[Co_2(R\text{-3-Cl-man})_2(bpy)_3](OTf)_2$ (**23R**); $[Co_2(R\text{-4-Cl-man})_2(bpy)_3](OTf)$ (**33R**); $[Co_2(R\text{-4-CH}_3\text{-man})_2(bpy)_3](OTf)_2$ (**43R**). These five CMOMs exhibit similar BET surface area and uptake for CO_2. However, we observed that the water sorption profiles of these CMOMs are different in terms of water uptake and pore-filling step. *In situ* infrared spectroscopy investigations were conducted upon water-loaded frameworks, and first-principles modelling revealed the preferred water binding sites and corresponding H-bond interactions.

a

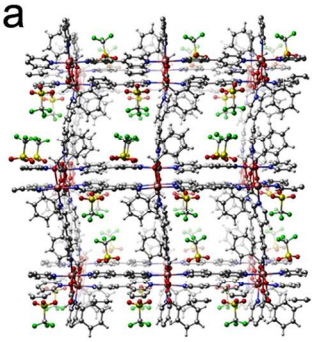

b

	3S	13R	23R	33R	43R
Metal	Co^{2+}	Co^{2+}	Co^{2+}	Co^{2+}	Co^{2+}
Spacer	bpy	bpy	bpy	bpy	bpy
Linker	(*S*)-man	(*R*)-2-Cl-man	(*R*)-3-Cl-man	(*R*)-4-Cl-man	(*R*)-4-Me-man
Anion	OTf^-	OTf^-	OTf^-	OTf^-	OTf^-

Figure 1. The five isostructural CMOMs with **bnn** topology studied herein. (a) Crystal structure of CMOM-**3S** as a representative. Color codes: C grey, O red, N blue, F green, S yellow, H white. (b) Components for the construction of CMOM-**3S**, **13R**, **23R**, **33R**, and **43R**. The structures are sustained by enantiopure mandelate (man) linkers and 4,4'-bipyridine (bpy) ligands.

RESULTS AND DISCUSSION

Single crystals of **3S**, **13R**, **23R**, **33R** and **43R** were prepared by solvent diffusion between MeOH solutions of $Co(OTf)_2 \cdot 6H_2O$ and the appropriate enantiopure mandelic acid layered over 1,2-dichlorobenzene or trifluorotoluene solutions of bpy. Single crystal X-ray diffraction studies of these CMOMs revealed that all five variants exhibit **bnn** topology (Figures 1 and S1). Four crystallized in chiral space group $P2_1$ whereas **23R** crystallized in $P2_12_12_1$ (Table S1). Pore chemistry, size and shape is in effect controlled by the mandelate substituents and the orientation of the OTf counterions, resulting in hourglass pore surfaces of the type seen in **1S** and **1R**.[15a] The maximum pore size of the 1D channels in these CMOMs is limited by the length of the bpy linkers and the cross-section is ca. 0.8 × 0.8 nm after subtracting van der Waals radii.

In **13R**, Cl atoms lie between two bpy ligands and orient towards an adjacent channel (Figure S1b) whereas substituents at the 3- and 4- positions only impact their own channels. Halogen-halogen interactions exist in **23R** and the phenyl rings tilt at an angle of ~36° (Figure S1c). This also results in doubling of the unit cell and adoption of the orthorhombic crystal system. Reduction of pore size is observed in **33R** and **43R** because of the alignment of -Cl and $-CH_3$ moieties in the channels. The void volume of the pores calculated using PLATON[17] was determined to be 25% (**3S**), 24% (**13R**) and 22% (**23R**, **33R**, and **43R**) of the unit cell volume. Powder X-ray diffraction (PXRD) patterns of as-synthesized CMOMs closely match those calculated from single crystal data (Figures S2-S6). Thermogravimetric analysis revealed 10%-20% weight loss upon initial heating and thermal stability to around 300 °C (Figure S7). Replacing nitrates in **1S** to triflates in the **3S** series enhanced thermal stability. The pore aperture of these CMOMs is affected by both the OTf anions and the phenyl moieties, both of which can adapt different positions. This suggested to us the possibility that these materials might serve as 4th generation "hard-soft" materials[12] through self-switching of pore size and chemistry. Unlike 3rd generation soft porous materials, which can breathe or swell with large unit cell differences, movement of OTf anions (Scheme 2d) and phenyl groups (Scheme 2e) would enable pore size and pore chemistry to adapt to guest molecules while the framework remains rigid. Our experiments reveal that such self-modification indeed happens.

As-synthesized crystals were activated for gas sorption studies by exchanging with DCM daily for 5 days and degassing under dynamic vacuum at room temperature for 24h. The permanent porosity of CMOMs was characterized by CO_2 sorption isotherms collected at 195 K (Figure S8). Uptakes of 83, 75, 86, 85, 82 cm^3 g^{-1} for **3S**, **13R**, **23R**, **33R**, and **43R** were observed, respectively. The specific surface areas calculated by the Brunauer–Emmett–Teller (BET) equation are 281, 293, 267, 241 and 203 m^2/g, respectively. Unlike earlier studies conducted upon MOFs based upon substituted ligands,[18] no significant changes in CO_2 uptake were observed at 195K. A steep jump in uptake for **33R** and **43R** at low partial pressure from 0.12 to 0.16 bars suggests that a pore size/chemistry change could indeed be induced by the OTf anions and phenyl groups.

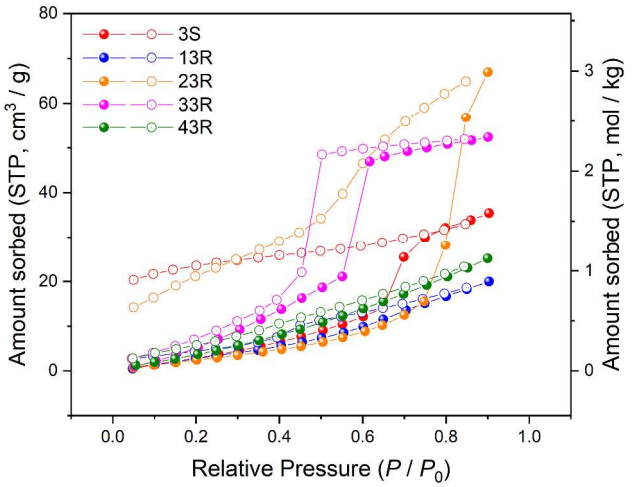

Figure 2. Water vapor adsorption (filled circle) and desorption (open circle) isotherms collected at 298K.

Water vapor isotherms were measured at ambient temperature (Figures 2, S9). The substituted mandelate linker ligands enabled significant variation in water sorption behavior. **13R** and **43R** exhibit very little water uptake over the entire relative pressure range, indicating hydrophobicity and/or pore blockage.[19] No significant hysteresis is observed for **13R** and **43R** in the desorption process. Conversely, **33R** has a water sorption isotherm that shows little water uptake up to $P/P_0 = 0.55$, followed by a steep adsorption and the maximum uptake of 52 cm^3 g^{-1} at $P/P_0 = 0.55$ along with a hysteresis loop. Similar steep increases in uptake were also observed by **3S** and **23R**, at which the relative pressures shifted from 0.55 to 0.65 and 0.75, respectively, along with hysteresis in the desorption pro-

cesses. The amount of water adsorbed in CMOMs varied from 20 to 67 $cm^3\ g^{-1}$ at nearly saturated pressure (P/P_0 = 0.9), and does not correlate with the respective surface areas. However, relatively high water loadings for **3S** and **23R** were measured at low relative pressures in the desorption process.

Unlike many MOFs that collapse after exposure to water vapor,[20] the CMOMs studied herein are stable to humidity as confirmed by PXRD (Figures S2-S6). The experimental PXRD patterns reveal that whereas peak intensities change between activated and gas-loaded samples, in some cases significantly, peak positions are retained. These results indicate framework rigidity, an expected feature of 4th generation materials. CMOMs also pass accelerated stability testing conditions of 75% humidity at 40°C for 7 days.[21] BET surface area analysis of reactivated CMOMs after incubation (Figure S10) revealed that **13R**, **33R** and **43R** retained their CO_2 sorption performance when compared to that of pristine samples. **3S** and **23R** were found to exhibit decreased BET surface area and less CO_2 uptake at 195K, which is consistent with the observation of retained water loading after desorption (Figure 2).

Table 1. Summary of phonon modes changes upon hydration of 33R up to ~11 Torr at room temperature

Phonon modes	Original position / cm^{-1}	Frequency shift at 11 Torr / cm^{-1}
$\nu(CH)_{phenyl}$	3070	+8
$\nu(CH)_{methyl}$	2938	+6
$\nu(CC)_{i.p.ring.\ bpy}$	1534	0
$\sigma(CH)_{def.\ bpy}$	1492	0
$\nu_s(COO)$	1416	0
$\nu_{as}(SO_3)$	1286	-4
$\nu_s(CF_3)$	1221	-10
$\nu_{as}(CF_3)$	1178	-10
$\nu_s(SO_3)$	1026	+6
$\sigma(CH)_{o.p.\ bpy}$	811	+2
ν(C-Cl)	781	+2
$\delta_{as}(SO_3)$	638	+6

Understanding the water sorption processes is essential for gaining an insight into the water binding sites in order to enable design of the next generation of sorbents. We therefore applied *in situ* techniques and modelling to structurally and physicochemically characterize guest-loaded frameworks to provide information about water molecule location and binding affinity.[22] IR spectroscopy can detect water adsorption states and probe structural changes upon loading water in MOFs.[22-23] Measurements were performed on all five samples by introducing H_2O vapor into the cell as a function of pressure from ~2 to 11 Torr (0.084 to 0.463 P/P_0), above which water condenses onto the KBr pellet. Based on the adsorption isotherm measurement, a steep increase of water uptake occurs in **33R** at 11 Torr. To identify and interpret any structural changes, a detailed assignment of the CMOM vibrational modes is necessary and was accomplished by comparing the spectra of triflate, pure mandelic acid ligand and bpy (see Table 1 for the selected assignment of **33R** modes and corresponding spectrum in bottom panel of Figure 3).

Upon loading water from 2 to 11 Torr into the activated CMOMs, no shift of coordinated carboxylate group is consistent with framework rigidity (Table 1). Conversely, significant change in the $\nu_s(COO)$ band is commonly observed in 3rd generation materials that contain carboxylate linkers.[12a] The stretching ν(OH) band of channel-adsorbed water is present in the difference spectra above 3000 cm^{-1} and the bending $\beta(OH_2)$ mode appears at around 1640 cm^{-1} (middle panel of Figures 3 and S9). A sharp mode appears at 3683 cm^{-1} at low pressure in **33R** and slightly red shifts to 3675 cm^{-1} at ~11 Torr. This mode, also observed in the other four CMOMs, can be assigned to a free OH stretching mode that is not involved in hydrogen bonding.[24] Another strong band at lower frequencies at 3514 cm^{-1} in **33R**, 3520 cm^{-1} in **43R**, 3541 cm^{-1} in **13R**, 3524 cm^{-1} at **23R**, and 3528 cm^{-1} in **3S** is assigned to the OH stretching mode of water molecules with very weak hydrogen bonding. Together with the growth of the water modes, the triflate modes are also perturbed (middle panel of Figure 3), including the stretching modes $\nu_{as}(SO_3)$ at ~1286 cm^{-1} and $\nu_s(SO_3)$ at ~1026 cm^{-1}, the bending mode of $\delta_s(SO_3)$ at 638 cm^{-1}, and the stretching modes $\nu_s(CF_3)$ at 1221 cm^{-1} and $\nu_{as}(CF_3)$ at 1178 cm^{-1}. These observations suggest that water molecules directly interact with triflate anions in the pore channels. At ~11 Torr, a dramatic increase of water adsorption was evidenced by the increase of both its stretching and bending bands (middle panel of Figure 3). In addition to changes in the water bands, the perturbations of the triflate modes of **33R** increase much more than those in the other four CMOMs (see Figure 3 and Figure S11), indicating a stronger interaction between water and triflate ions in **33R** (*vide infra*). Besides the perturbation of triflate, there is a change in the absorption spectrum of mandelate in **33R** induced by water adsorption. Firstly, the stretching mode ν of CH from the aromatic ring and methylene groups around 3000 cm^{-1} is strongly perturbed in **33R** but remains unaffected in the other four CMOMs. Another notable change in the difference spectra of **33R** is evident around 700 cm^{-1}, which would be assigned to the perturbation of the benzene ring deformation mode σ(CCC) of mandelate. This change is also absent in the spectra of the other CMOMs. All these observations point to a structural transformation of triflate anions and phenyl groups in **33R** induced by the presence of water above 11 Torr.

The perturbation of the triflate modes in all five CMOMs induced by water inclusion into the frameworks suggests that water preferentially interacts mainly with triflate anions. It has been reported that a ν(OH) band above 3660 cm^{-1} was observed in solid hydrates $La(CF_3SO_3)_3{\cdot}xH_2O$, $Na(CF_3CO_2){\cdot}xH_2O$ and their concentrated solutions.[25] This sharp band, distinguishable from bulk hydrogen bonded water molecules, can be interpreted as originating from water screened by the CF_3 end of the $CF_3SO_3^-$. Therefore, it is reasonable to conclude that the sharp bands above 3670 cm^{-1} in CMOMs originate from isolated water molecules next to triflate anions. The CH bending mode of bpy at 810 cm^{-1} is also shifted after water adsorption, indicating that adsorbed water molecules perturb the bpy linker by its oxygen atom interacting with the C-H of the pyridyl ring. Differential spectra presented in the top panel of Figure 3 provide further information on the adsorbed water state upon increasing water vapor pressure to ~11 Torr. The spectrum was obtained by subtracting the IR spectrum of adsorbed H_2O from the one at the previous pressure point (middle panel of Figure 3). Below 9 Torr, the peaks of water stretching bands grow in a similar trend, indicating a gradual occupation of each single adsorption site. Between 11 Torr and 9 Torr broadening of the OH stretching band above 3000 cm^{-1} occurs. The bending mode $\beta(H_2O)$ also broadens and shifts by 10 cm^{-1}, indicating that aggregation of water mole-

cules through hydrogen bonding had then occured.[26] This is consistent with the experimental isotherm measurement that water uptake steeply increases above ~11 Torr in **33R**. The broadening and shift of both stretching and bending bands in the differential spectra are absent in the other four materials.

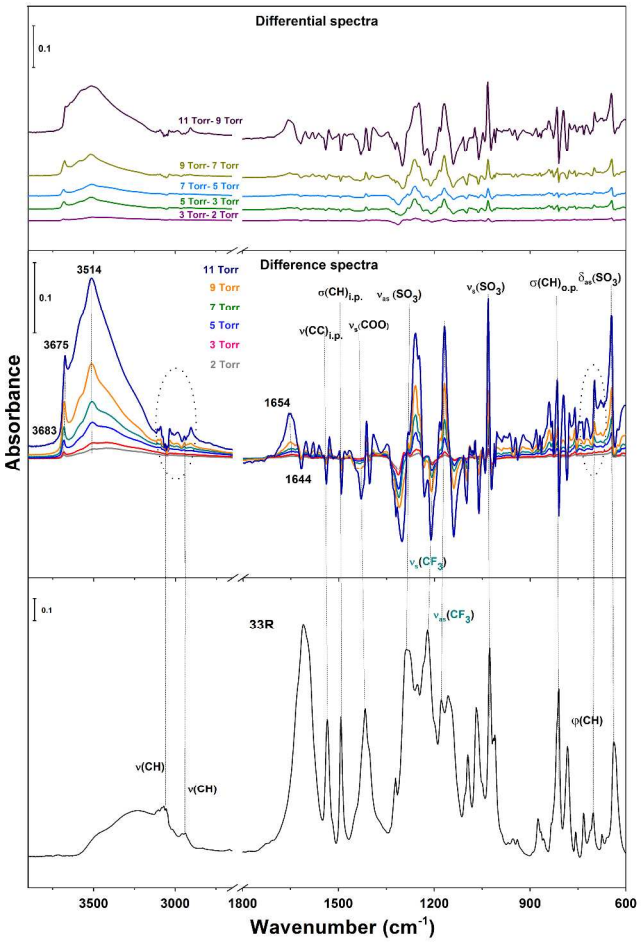

Figure 3. Top panel: differential spectra showing the increase of water bands with the pressure increase, each spectrum was referenced to previous data collected at lower pressure; middle panel: difference spectra of H_2O adsorbed into 33R as a function of water vapour pressure (bottom), referenced to activated 33R in vacuum (<20 mTorr base pressure); bottom: IR spectra of activated 33R, reference to pure KBr pellet in vacuum (<20 mTorr base pressure).

In order to validate the water adsorption sites, first-principle calculations were conducted on the desolvated **13R**, **33R**, and **43R** structures. Our first-principle calculations were performed at the density functional theory (DFT) level using VASP[27] with the vdW-DF exchange-correlation functional.[28] The ground state relaxed structures indicate no significant difference of the orientation of the mandelate linkers in the unperturbed **13R**, **33R**, and **43R** structures after removing the solvent.

The main structural difference between the CMOMs studied herein is the substitution of the mandelate ligands. The spectroscopic evidence points to the possibility of a structural rearrangement of triflate anions in all CMOMs and the phenyl groups at ~11 Torr only in **33R**. To analyze the effect of water on the structural changes of CMOMs, a water molecule was added to find the probable binding sites. Several potential sites in close proximity to the mandelate linker and triflate anions were tested. Consistent with the spectroscopic indication that water mostly interacts with triflate anions in all three CMOMs, we found that the water molecule binds to the triflate anion via a hydrogen bond to the oxygen of the sulfate group. The configuration of the water molecule is affected by the mandelate functionality; for example, in **33R**, the non-interacting H is oriented towards the neighboring methyl moiety. This binding causes a rearrangement of the triflate anion as it rotates slightly and moves position (Table S3), thereby explaining the observed perturbation of $\nu_{as}(SO_3)$, $\nu_s(SO_3)$, $\delta_s(SO_3)$ $\nu_s(CF_3)$ and $\nu_{as}(CF_3)$ modes in Figure 3. The water molecule is confined within the channel and its interactions with other parts of the CMOM cavity produce a sharp OH stretching mode in the IR spectra. The rest of the structure, including bpy and mandelate, remain only slightly affected, which is consistent with the spectroscopic observation that these modes are not obviously perturbed.

The binding energy of water varies only slightly between the three structures and shows no clear distinction to indicate why **33R** uptakes H_2O while **13R** and **43R** do not. We found that **13R** has the strongest binding, followed by **43R**, and then **33R** but with variances of only 3-5 %. To further understand the nature of the water interaction, we also tested the binding strength of water to the framework without the presence of the interacting triflate anion as well as how the water binds to the triflate anion in the absence of the framework. The binding strengths are summarized in Table S2. A water molecule will bind to the isolated triflate anion with a strength of –0.278 eV, which is weaker than the water binding to the full CMOM system. Additionally, the binding strength of the water to the CMOM structures in the absence of the interacting triflate anion tells us that water would bind to the CMOM structure for the chlorinated systems of **13R** and **33R**, but the **43R** system is hydrophobic as water binding is unfavorable.

Bond distances for the various interactions of the water, CMOM, and triflate anion are presented in Table S3. The most interesting interaction happens when comparing the distance of the triflate anion to the CMOM structure at the point of the hydrogen bond between the triflate oxygen and OH of the mandelate. Upon addition of water, the hydrogen bond distance increases for the **13R** and **43R** structures but decreases in the **33R** structure. The most drastic case is **13R** where the distance increases by 0.4 Å. However, the presence of one water molecule in these structures does not affect the pore size in comparison of those of the ground state (Table S4).

To further understand how water molecules affect the CMOM structures and the nature of the binding, charge rearrangement upon binding was calculated. The charge rearrangement was calculated by subtracting the charge density of the isolated CMOM structure and the isolated water molecule from the charge density of the water bound to the CMOM structure. Figure 4 shows the rearrangement for each structure. The blue and yellow lobes around the atoms and molecules indicate a change in charge distribution due to binding. The most likely explanation for the disparity of water uptake is that water is affecting the nature of the hydrogen bond between the triflate anion and the OH of the mandelate. All three models show expected charge rearrangement of the water molecule and triflate anion; however, in the **33R** structure, water binding affects the triflate to a much greater extent than for **13R** and **43R**. **43R** shows near zero charge rearrangement on the

carboxylate and mandelic functional upon addition of the water molecule (Figure 4b). The chlorinated mandelate ligands of **33R** and **13R** show slight charge rearrangement upon binding of the H_2O. Taking into account the much more prevalent charge redistribution found in **33R** along with the hydrogen bond distance between the triflate and OH of the mandelate shortens, it is likely the water is having a much more drastic effect on the structure of **33R** structure than **13R** and **43R**.

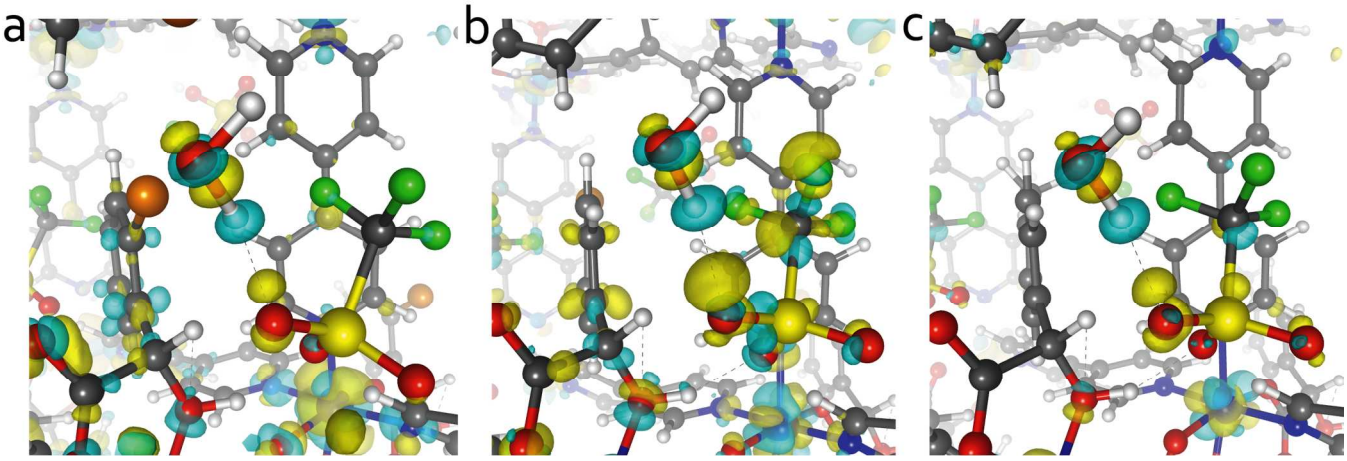

Figure 4. Charge redistribution upon binding H_2O in CMOM-**13R** (a), **33R** (b), **43R** (c) structures, focusing at the interaction of the H_2O-OTf with the carboxylate of the mandelate. Blue color indicates a loss of charge and yellow color a gain of charge upon binding. Atoms colored as follows: C grey, O red, N blue, H white, Co pink, S yellow, F green, and Cl orange. Visualization was done at an isosurface value of $3x10^{-3}$ e/Å^3.

CONCLUSION

In summary, the CMOMs reported herein represent examples of a new type of 4th generation "hard-soft" porous material resulting from the inherent flexibility of phenyl groups and the ability extra-framework triflate anions to rearrange their lattice positions. The outcome is pore size and chemistry that can adapt to accommodate guest molecules while the framework remains rigid. In a previous study we revealed that the parent material **3S** can take advantage of its inherent chirality and its soft pores to selectively bind chiral alcohols.[15b] Herein, we have demonstrated that the self-switching nature of an isostructural family of these materials enables them to adsorb water molecules in varying ways. In particular, distinctive water uptake and pore filling pressures were observed in the five isostructural CMOMs studied herein. *In situ* IR characterization and theoretical simulations revealed that water molecules are involved in various hydrogen bonding interactions and that the extra-framework triflate anions are engaged in these interactions. Overall, we were able to modulate water sorption. We consider these results to be broadly relevant in that they suggest that 4th generation porous materials are well-suited to modulate other relevant vapor and gas sorption processes.

ASSOCIATED CONTENT

Supporting Information. Experimental and computational details, additional figures and tables. This material is available free of charge via the Internet at http://pubs.acs.org.

AUTHOR INFORMATION

Corresponding Author

* xtal@ul.ie

ACKNOWLEDGMENT

This work was supported by the Science Foundation of Ireland (Award 13/RP/B2549). Work in the US was supported in full by the Department of Energy, Basic Energy Sciences, division of Materials Sciences and Engineering (DOE Grant No. DE-FG02-08ER46491).

REFERENCES

(1) (a) Hepbasli, A.; Kalinci, Y. *Renew. Sust. Energ. Rev.* **2009**, *13*, 1211; (b) Meunier, F. *Appl. Therm. Eng.* **2013**, *61*, 830; (c) Khutia, A.; Rammelberg, H. U.; Schmidt, T.; Henninger, S.; Janiak, C. *Chem. Mater.* **2013**, *25*, 790.

(2) (a) Seo, Y.-K.; Yoon, J. W.; Lee, J. S.; Hwang, Y. K.; Jun, C.-H.; Chang, J.-S.; Wuttke, S.; Bazin, P.; Vimont, A.; Daturi, M.; Bourrelly, S.; Llewellyn, P. L.; Horcajada, P.; Serre, C.; Férey, G. *Adv. Mater.* **2012**, *24*, 806; (b) Guo, P.; Wong-Foy, A. G.; Matzger, A. J. *Langmuir* **2014**, *30*, 1921; (c) AbdulHalim, R. G.; Bhatt, P. M.; Belmabkhout, Y.; Shkurenko, A.; Adil, K.; Barbour, L. J.; Eddaoudi, M. *J. Am. Chem. Soc.* **2017**, *139*, 10715.

(3) (a) Park, K.-C.; Chhatre, S. S.; Srinivasan, S.; Cohen, R. E.; McKinley, G. H. *Langmuir* **2013**, *29*, 13269; (b) Kim, H.; Yang, S.; Rao, S. R.; Narayanan, S.; Kapustin, E. A.; Furukawa, H.; Umans, A. S.; Yaghi, O. M.; Wang, E. N. *Science* **2017**, *356*, 430.

(4) (a) Khan, N. A.; Jung, B. K.; Hasan, Z.; Jhung, S. H. *J. Hazard. Mater.* **2015**, *282*, 194; (b) Kovalova, L.; Knappe, D. R. U.; Lehnberg, K.; Kazner, C.; Hollender, J. *Environ. Sci. Pollut. Res.* **2013**, *20*, 3607; (c) Alsbaiee, A.; Smith, B. J.; Xiao, L.; Ling, Y.; Helbling, D. E.; Dichtel, W. R. *Nature* **2015**, *529*, 190; (d) Ding, S.-Y.; Dong, M.; Wang, Y.-W.; Chen, Y.-T.; Wang, H.-Z.; Su, C.-Y.; Wang, W. *J. Am. Chem. Soc.* **2016**, *138*, 3031; (e) Sun, Q.; Aguila, B.; Perman, J.; Earl, L. D.; Abney, C. W.; Cheng, Y.; Wei, H.; Nguyen, N.; Wojtas, L.; Ma, S. *J. Am. Chem. Soc.* **2017**, *139*, 2786.

(5) (a) Wang, C.; Liu, X.; Keser Demir, N.; Chen, J. P.; Li, K. *Chem. Soc. Rev.* **2016**, *45*, 5107; (b) Canivet, J.; Fateeva, A.; Guo, Y.; Coasne, B.; Farrusseng, D. *Chem. Soc. Rev.* **2014**, *43*, 5594.

(6) Furukawa, H.; Gándara, F.; Zhang, Y.-B.; Jiang, J.; Queen, W. L.; Hudson, M. R.; Yaghi, O. M. *J. Am. Chem. Soc.* **2014**, *136*, 4369.

(7) (a) Kizzie, A. C.; Wong-Foy, A. G.; Matzger, A. J. *Langmuir* **2011**, *27*, 6368; (b) Yu, K.; Kiesling, K.; Schmidt, J. R. *J. Phys. Chem. C* **2012**, *116*, 20480.

(8) (a) Batten, S. R.; Neville, S. M.; Turner, D. R. *Coordination polymers: design, analysis and application*; Royal Society of Chemistry, 2009; (b) Kitagawa, S.; Kitaura, R.; Noro, S. i. *Angew. Chem. Int. Ed.* **2004**, *43*, 2334.

(9) (a) MacGillivray, L. R. *Metal-organic frameworks: design and application*; John Wiley & Sons, 2010; (b) Zhou, H.-C.; Long, J. R.; Yaghi, O. M. *Chem. Rev.* **2012**, *112*, 673.

(10) (a) Nugent, P.; Belmabkhout, Y.; Burd, S. D.; Cairns, A. J.; Luebke, R.; Forrest, K.; Pham, T.; Ma, S.; Space, B.; Wojtas, L.; Eddaoudi, M.; Zaworotko, M. J. *Nature* **2013**, *495*, 80; (b) Zheng, J.; Vemuri, R. S.; Estevez, L.; Koech, P. K.; Varga, T.; Camaioni, D. M.; Blake, T. A.; McGrail, B. P.; Motkuri, R. K. *J. Am. Chem. Soc.* **2017**, *139*, 10601; (c) Eddaoudi, M.; Kim, J.; Rosi, N.; Vodak, D.; Wachter, J.; O'Keeffe, M.; Yaghi, O. M. *Science* **2002**, *295*, 469; (d) Chen, B.; Xiang, S.; Qian, G. *Acc. Chem. Res.* **2010**, *43*, 1115; (e) Zheng, B.; Bai, J.; Duan, J.; Wojtas, L.; Zaworotko, M. J. *J. Am. Chem. Soc.* **2011**, *133*, 748.

(11) Kitagawa, K.; Kondo, M. *Bull. Chem. Soc. Jpn.* **1998**, *71*, 1739.

(12) (a) Schneemann, A.; Bon, V.; Schwedler, I.; Senkovska, I.; Kaskel, S.; Fischer, R. A. *Chem. Soc. Rev.* **2014**, *43*, 6062; (b) Ferey, G.; Serre, C. *Chem. Soc. Rev.* **2009**, *38*, 1380; (c) Horike, S.; Shimomura, S.; Kitagawa, S. *Nat. Chem.* **2009**, *1*, 695; (d) Bennett, T. D.; Cheetham, A. K.; Fuchs, A. H.; Coudert, F.-X. *Nat. Chem.* **2016**, *9*, 11; (e) Yang, Q.-Y.; Lama, P.; Sen, S.; Lusi, M.; Chen, K.-J.; Gao, W.-Y.; Shivanna, M.; Pham, T.; Hosono, N.; Kusaka, S.; Perry, J.J.P.; Ma, S.-Q.; Space, B.; Barbour, L.J.; Kitagawa, S.; Zaworotko, M.J. *Angew. Chem. Int. Ed.* **2018**, *57*, 5684. (f) Kitagawa, S. *New Dimensions of Porous Coordination Polymers/Metal-Organic Frameworks*, Abstract A00584-SK, 43rd International Conference on Coordination Chemistry, Sendai, Japan, July 30th-August 4th 2018.

(13) Liu, J.; Chen, L.; Cui, H.; Zhang, J.; Zhang, L.; Su, C.-Y. *Chem. Soc. Rev.* **2014**, *43*, 6011.

(14) (a) Wang, Z.; Cohen, S. M. *Chem. Soc. Rev.* **2009**, *38*, 1315; (b) Cohen, S. M. *Chem. Rev.* **2011**, *112*, 970; (c) Cohen, S. M. *J. Am. Chem. Soc.* **2017**, *139*, 2855.

(15) (a) Zhang, S.-Y.; Wojtas, L.; Zaworotko, M. J. *J. Am. Chem. Soc.* **2015**, *137*, 12045; (b) Zhang, S.-Y.; Yang, C.-X.; Shi, W.; Yan, X.-P.; Cheng, P.; Wojtas, L.; Zaworotko, M. J. *Chem* **2017**, *3*, 281.

(16) Inokuma, Y.; Yoshioka, S.; Ariyoshi, J.; Arai, T.; Hitora, Y.; Takada, K.; Matsunaga, S.; Rissanen, K.; Fujita, M. *Nature* **2013**, *495*, 461.

(17) Spek, A. *J. Appl. Cryst.* **2003**, *36*, 7.

(18) (a) Akiyama, G.; Matsuda, R.; Sato, H.; Hori, A.; Takata, M.; Kitagawa, S. *Microporous Mesoporous Mater.* **2012**, *157*, 89; (b) Reinsch, H.; van der Veen, M. A.; Gil, B.; Marszalek, B.; Verbiest, T.; de Vos, D.; Stock, N. *Chem. Mater.* **2013**, *25*, 17; (c) Jasuja, H.; Burtch, N. C.; Huang, Y.-g.; Cai, Y.; Walton, K. S. *Langmuir* **2013**, *29*, 633; (d) Behrens, K.; Mondal, S. S.; Nöske, R.; Baburin, I. A.; Leoni, S.; Günter, C.; Weber, J.; Holdt, H.-J. *Inorg. Chem.* **2015**, *54*, 10073.

(19) (a) Burtch, N. C.; Jasuja, H.; Walton, K. S. *Chem. Rev.* **2014**, *114*, 10575; (b) Bai, Y.; Dou, Y.; Xie, L.-H.; Rutledge, W.; Li, J.-R.; Zhou, H.-C. *Chem. Soc. Rev.* **2016**, *45*, 2327.

(20) (a) Küsgens, P.; Rose, M.; Senkovska, I.; Fröde, H.; Henschel, A.; Siegle, S.; Kaskel, S. *Microporous Mesoporous Mater.* **2009**, *120*, 325; (b) Cychosz, K. A.; Matzger, A. J. *Langmuir* **2010**, *26*, 17198.

(21) Kumar, A.; Madden, D. G.; Lusi, M.; Chen, K.-J.; Daniels, E. A.; Curtin, T.; Perry, J. J.; Zaworotko, M. J. *Angew. Chem. Int. Ed.* **2015**, *54*, 14372.

(22) (a) Vaidhyanathan, R.; Iremonger, S. S.; Shimizu, G. K. H.; Boyd, P. G.; Alavi, S.; Woo, T. K. *Science* **2010**, *330*, 650; (b) Yang, S.; Sun, J.; Ramirez-Cuesta, A. J.; Callear, S. K.; DavidWilliam, I. F.; Anderson, D. P.; Newby, R.; Blake, A. J.; Parker, J. E.; Tang, C. C.; Schröder, M. *Nat. Chem.* **2012**, *4*, 887; (c) Easun, T. L.; Moreau, F.; Yan, Y.; Yang, S.; Schroder, M. *Chem. Soc. Rev.* **2017**, *46*, 239; (d) McDonald, T. M.; Mason, J. A.; Kong, X.; Bloch, E. D.; Gygi, D.; Dani, A.; Crocellà, V.; Giordanino, F.; Odoh, S. O.; Drisdell, W. S.; Vlaisavljevich, B.; Dzubak, A. L.; Poloni, R.; Schnell, S. K.; Planas, N.; Lee, K.; Pascal, T.; Wan, L. F.; Prendergast, D.; Neaton, J. B.; Smit, B.; Kortright, J. B.; Gagliardi, L.; Bordiga, S.; Reimer, J. A.; Long, J. R. *Nature* **2015**, *519*, 303; (e) Hoffmann, H.; Debowski, M.; Müller, P.; Paasch, S.; Senkovska, I.; Kaskel, S.; Brunner, E. *Materials* **2012**, *5*, 2537; (f) Tan, K.; Zuluaga, S.; Gong, Q.; Canepa, P.; Wang, H.; Li, J.; Chabal, Y. J.; Thonhauser, T. *Chem. Mater.* **2014**, *26*, 6886; (g) Tan, K.; Canepa, P.; Gong, Q.; Liu, J.; Johnson, D. H.; Dyevoich, A.; Thallapally, P. K.; Thonhauser, T.; Li, J.; Chabal, Y. J. *Chem. Mater.* **2013**, *25*, 4653; (h) Tan, K.; Zuluaga, S.; Fuentes, E.; Mattson, E. C.; Veyan, J.-F.; Wang, H.; Li, J.; Thonhauser, T.; Chabal, Y. J. *Nat. Commun.* **2016**, *7*, 13871.

(23) Nijem, N.; Canepa, P.; Kaipa, U.; Tan, K.; Roodenko, K.; Tekarli, S.; Halbert, J.; Oswald, I. W. H.; Arvapally, R. K.; Yang, C.; Thonhauser, T.; Omary, M. A.; Chabal, Y. J. *J. Am. Chem. Soc.* **2013**, *135*, 12615.

(24) Vimont, A.; Goupil, J.-M.; Lavalley, J.-C.; Daturi, M.; Surblé, S.; Serre, C.; Millange, F.; Férey, G.; Audebrand, N. *J. Am. Chem. Soc.* **2006**, *128*, 3218.

(25) (a) Bergström, P.-Å.; Lindgren, J. *J. Mol. Struct.* **1991**, *245*, 221; (b) Bergström, P.-Å.; Lindgren, J. *J. Mol. Struct.* **1990**, *239*, 103.

(26) (a) Brubach, J.-B.; Mermet, A.; Filabozzi, A.; Gerschel, A.; Roy, P. *J. Chem. Phys.* **2005**, *122*, 184509; (b) Bellissent-Funel, M. C. *J. Phys.: Condens. Matter* **2001**, *13*, 9165; (c) Nalaparaju, A.; Babarao, R.; Zhao, X. S.; Jiang, J. W. *ACS Nano* **2009**, *3*, 2563.

(27) (a) Kresse, G.; Furthmüller, J. *Phy. Rev. B* **1996**, *54*, 11169; (b) Kresse, G.; Joubert, D. *Phy. Rev. B* **1999**, *59*, 1758.

(28) (a) Thonhauser, T.; Zuluaga, S.; Arter, C. A.; Berland, K.; Schröder, E.; Hyldgaard, P. *Phy. Rev. Lett.* **2015**, *115*, 136402; (b) Kristian, B.; Valentino, R. C.; Kyuho, L.; Elsebeth, S.; Thonhauser, T.; Per, H.; Bengt, I. L. *Rep. Prog. Phys.* **2015**, *78*, 066501; (c) Langreth, D. C.; Lundqvist, B. I.; Chakarova-Käck, S. D.; Cooper, V. R.; Dion, M.; Hyldgaard, P.; Kelkkanen, A.; Kleis, J.; Lingzhu, K.; Shen, L.; Moses, P. G.; Murray, E.; Puzder, A.; Rydberg, H.; Schröder, E.; Thonhauser, T. *J. Phys. Condens. Matter* **2009**, *21*, 084203; (d) Thonhauser, T.; Cooper, V. R.; Li, S.; Puzder, A.; Hyldgaard, P.; Langreth, D. C. *Phy. Rev. B* **2007**, *76*, 125112.

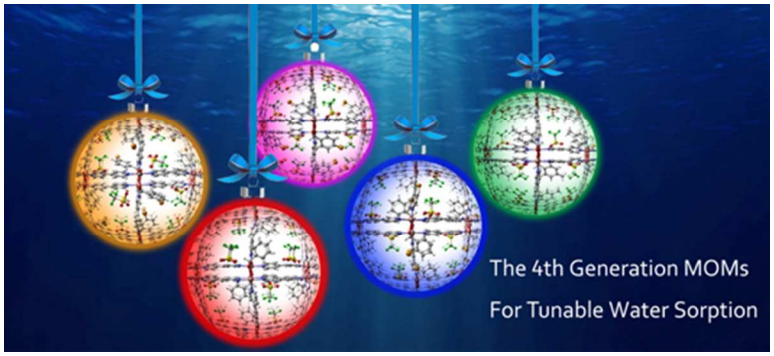
The 4th Generation MOMs
For Tunable Water Sorption